


## Research Article

# Intense $\gamma$ -Ray Bursts following the Interaction of Laser Pulse with Steep Density Gradients

S. Chintalwad,<sup>1</sup> S. Krishnamurthy,<sup>1</sup> S. Morris,<sup>2</sup> and B. Ramakrishna <sup>1</sup>

<sup>1</sup>Department of Physics, Indian Institute of Technology Hyderabad, Kandi, Sangareddy 502284, India

<sup>2</sup>Centre for Fusion, Space and Astrophysics, Department of Physics, University of Warwick, Coventry CV4 7AL, UK

Correspondence should be addressed to B. Ramakrishna; [bhuvan@phy.iith.ac.in](mailto:bhuvan@phy.iith.ac.in)

Received 1 April 2022; Revised 3 May 2022; Accepted 13 May 2022; Published 18 June 2022

Academic Editor: Wang Xinxin

Copyright © 2022 S. Chintalwad et al. This is an open access article distributed under the Creative Commons Attribution License, which permits unrestricted use, distribution, and reproduction in any medium, provided the original work is properly cited.

We investigate the production of intense  $\gamma$ -rays following the interaction of ultraintense laser pulse with a hybrid combination of under-dense plasma associated with a thin foil of fully ionized Al or Cu or Au at the rear side. Relativistic electrons are accelerated following the interaction of high intensity laser pulses with an under-dense plasma. These electrons are then stopped by the thin foils attached to the rear side of the under-dense plasma. This results in the production of intense-ray bursts. So, the enhancement of photon generation is due to the under-dense plasma electrons interacting with different over-dense plasma. Using open-source PIC code EPOCH, we study the effect of different electron densities in the under-plasma on photon emission. Photon emission enhancement is observed by increasing the target  $Z$  in the hybrid structure. Hybrid structure can enhance photon emission; it can increase the photon energy and yield and improve photon beam divergence. Simulations were also performed to find the optimal under-dense plasma density for  $\gamma$ -ray production.

## 1. Introduction

Recent developments in laser intensities of the order of  $10^{22}$  to  $10^{23}$   $\text{Wcm}^{-2}$  are possible due to the production of femto-second pulses by the introduction of the Chirped Pulse Amplification (CPA) technique [1]. The increase in laser intensity [2] has advanced the fields related to science and technology. In particular, the laser-plasma interaction has been the frontier of research with regard to accelerator physics [3], radiography [4], radiation therapy [5], and laboratory astrophysics [6]. Relativistic electrons are accelerated to MeV energies with the currently available intense laser systems. The nonlinear processes [7] associated with these relativistic electrons lead to radiation ranging from X-rays to  $\gamma$ -rays. High-energy X-rays are employed for very high-resolution imaging such as Thomson scattering and high-energy sources. The bright  $\gamma$ -ray sources are also useful in nuclear physics related to waste management and in the production of  $\gamma$ - $\gamma$  colliders. [8], which are of fundamental importance to the science community. Besides using proton bunches generated from the ion acceleration in

the inertial confinement fusion (ICF) application [9–11], the bremsstrahlung radiation generated from laser wake field acceleration (LWFA) could also be used in ICF [12, 13]. Edward et al. [14] used laser-accelerated electrons in solid targets and under-dense plasma (gas-jet) to produce a highly collimated, high-flux beam. Radiography of complex and dense materials using  $\gamma$ -sources was demonstrated by Glinec et al. in 2005 [15]. However, such sources could not be employed in practical applications due to poor control of beam parameters such as divergence and energy controlling the beam quality must be improved. Such a compact  $\gamma$ -ray source can be used in industrial applications such as detector calibration and testing.

PET (positron emission tomography) is a radioisotope-based imaging technology used in cancer diagnosis [16]. Proton beams from conventional accelerators, such as LINAC, are generally used to produce radio isotopes. However, radioisotopes can also be produced by photo-nuclear processes arising from  $\gamma$ -ray irradiation. LWFA is a promising path for  $\gamma$ -ray-based radioisotope production which has emerged from current technology. This method

uses compact tabletop lasers over high-end particle accelerators which are inexpensive and accessible. Radioisotope activation with the  $\gamma$ -rays produced by the bremsstrahlung of LWFA electrons have been demonstrated by various experiments [17–19]. For practical applications, it is crucial to achieve the desired beam features such as the source size, divergence, and electron-photon conversion efficiency. Using conventional accelerators in the low-energy range, analysis of bremsstrahlung sources for target material and thickness was performed by Marzini et al. [20], and LWFA-based bremsstrahlung sources are a key advancement for laser plasma-based particle sources which can be used for various applications. On the other hand, the Direct Laser Acceleration (DLA) mechanism accelerates electrons by laser electromagnetic waves in the ion channel or the plasma bubble through betatron resonance. In (DLA), the electrons in the ion channel or the plasma bubble are imparted with much higher energy than in vacuum [21]. The (DLA) regime is also very attractive due to a wide variety of potential practical applications such as the production of the MeV range of ultrarelativistic electrons that can serve as compact X-ray radiation sources [22]. Apart from this, the (DLA) regime is also useful in novel sources of other energetic particles such as ions [23], neutrons [24], and positrons [25].

Recent studies have shown that the  $\gamma$ -rays produced by laser-driven bremsstrahlung [26–28] and Compton scattering or Thomson scattering [29–32] which are based on laser-wake field accelerators [33–36] can produce highly collimated and quasimonochromatic  $\gamma$ -rays. Bremsstrahlung is produced when a charged particle is stopped by the strong electric fields inside the atomic nuclei. When a laser interacts with a plasma, the emitted photon energy is determined by the laser's intensity, as well as target parameters such as thickness, atomic number, and the cross section of electron interaction with an atomic nucleus. The interaction of a high-intensity laser pulse with a target is divided into two steps: first, the laser-plasma interaction produces MeV electrons [37–39], and then, in a high  $Z$  solid target, the process of the production of bremsstrahlung when a high intensity laser pulse interacts with matter is basically due to the production of MeV electrons by laser and subsequent quenching of these electrons in the strong field of the atomic nuclei. The interaction cross section to produce bremsstrahlung radiation is increased with increase in  $Z$  of the target [40]. The processes involving the atomic nucleus, such as bremsstrahlung ( $e^- + Z \rightarrow (e^- + \gamma + Z)$ ), play an important role in the production of plasmas with a high charge state or/and large atomic number  $Z$ . The interaction of a high-energy electron bunch with a high- $Z$  target such as copper or gold is where bremsstrahlung radiation would be most important. With the help of high laser intensities, the bremsstrahlung may produce comparable amounts of  $\gamma$ -ray radiation. Laser Wake-Field Acceleration (LWFA) [41] or (DLA) mechanisms can accelerate electrons in under-dense plasma. In a double-layer interaction setup [42, 43], firstly, a high-intense laser pulse interacts with the under-dense plasma and accelerates hot electrons in the under-dense region by LWFA or DLA [44, 45], and then these accelerated electrons are stopped by the nuclear potential of the foil

target placed at the rear side of the under-dense region. Higher electron energy leads to more efficient  $\gamma$ -ray emission as the bremsstrahlung cross section increases with electron energy [46, 47]. In plasma, the bremsstrahlung emission is strongly dependent on the interaction cross section between the incoming electron and the nuclear potential of the target. Furthermore, the cross section depends on the  $Z$  of the target. The cross section ( $\sigma_b$ ) is proportional to  $\alpha r_e^2 Z^2$  where  $\alpha = e^2/\hbar c = 1/137$  is the fine structure constant and  $r_e = e^2/mc^2$  is the classical electron radius, respectively. The interaction cross section increases with increasing the  $Z$  of the target. For the Al ( $Z = 13$ ) target, interaction cross section has  $\sigma_b \approx 169\alpha r_e^2$ , for Cu target ( $Z = 29$ ), it is around  $\sigma_b \approx 841\alpha r_e^2$ , and for the Au target ( $Z = 79$ ), cross section will be  $\sigma_b \approx 6241\alpha r_e^2$  [48, 49].

In this paper, we investigate the photon emission by the bremsstrahlung mechanism; we use the open-source particle-in-cell (PIC) code EPOCH [50] for this study. The bremsstrahlung mechanism is studied using the Monte Carlo (MC) algorithm, which is already included in the EPOCH code [46]. We study the relative strength of the bremsstrahlung radiation for various densities of the under-dense plasma. When an ultra-intense laser with an intensity  $I = 4 \times 10^{21} \text{ W cm}^{-2}$  is used to irradiate the under-dense plasma with the density of  $0.02n_c$  to  $2n_c$ , by attaching fully ionized targets such as Al or Au or Cu to the rear side of the under-dense plasma, the effect of the rear side target electron density on the emission of  $\gamma$ -rays is discussed in detail.

## 2. Simulation Set-Up

The simulations were performed with the 2D PIC code EPOCH. The simulation box covers ( $0 \mu\text{m}$  to  $50 \mu\text{m}$ ) along the  $x$ -direction and ( $-10 \mu\text{m}$  to  $10 \mu\text{m}$ ) along the  $y$ -direction with  $5000 \times 2000$  cells with a cell size of  $10 \text{ nm}$  along the  $x$ -direction and  $y$ -direction. The under-dense hydrogen plasma with an electron density of ( $0.02n_c$  to  $2n_c$ ) is placed at  $1 \mu\text{m}$  to  $41 \mu\text{m}$  with  $40 \mu\text{m}$  thickness. Electrons and ions have 32 macroparticles per cell. A P-polarized laser pulse of wavelength  $0.8 \mu\text{m}$  with a focal spot radius of  $1 \mu\text{m}$  is used. The peak intensity is  $4 \times 10^{21} \text{ W cm}^{-2}$  with a pulse duration of FWHM 30 fs. The laser pulse has a Gaussian spatial and temporal profile. The laser pulse enters the simulation box from  $x = 0 \mu\text{m}$  left boundary at the start of the simulation ( $t = 0$ ), Al, or Cu, or Au with a thickness of  $1 \mu\text{m}$  attached to the rear side of the under-dense plasma has been considered as a fully ionized plasma with the electron density  $n_e = 455n_c$  for Al,  $n_e = 2238n_c$  for Cu, and  $n_e = 4234.4n_c$  for Au where  $n_c$  is electron critical density  $n_c = \epsilon_0 m_e \omega_0^2 / 4\pi e^2$  with laser frequency  $\omega_0 = 2\pi c/\lambda_0$  where  $\epsilon_0$ ,  $m_e$ ,  $e$ , and  $\lambda$  are permittivity of free space, the mass of an electron, electron charge, and laser wavelength, respectively. The critical density corresponding to the laser wavelength  $\lambda = 0.8 \mu\text{m}$  is  $n_c = 1.71 \times 10^{21} \text{ cm}^{-3}$ . Only photons with energies greater than 50 keV are considered in all simulations. For computational convenience and in order to look into only the high-energy photons, we have considered only those photons with energy above 50 keV. The interaction set-up for double layer simulation is shown in Figure 1.

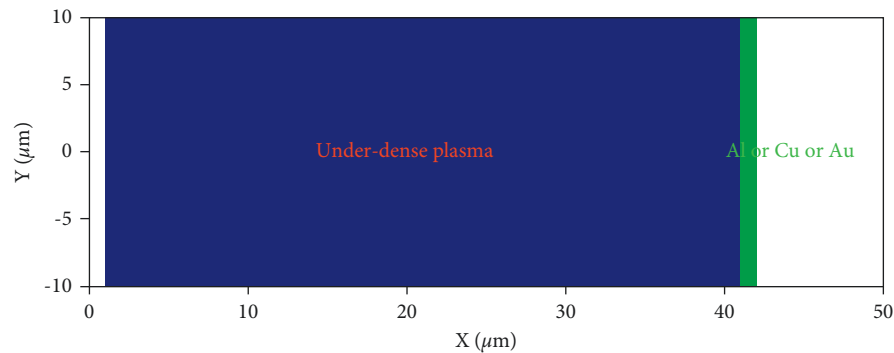


FIGURE 1: Simulation interaction set-up.

### 3. Results and Discussions

To study the photon emission in this double layer interaction setup, firstly, the interaction of a laser pulse with a  $40\ \mu\text{m}$  thick under-dense hydrogen plasma containing electrons and protons with a density of  $0.2n_c$  is considered. The interaction of ultraintense laser pulses with various under-dense plasma densities is then compared. The simulation results showing the electron density in under-dense plasma and corresponding electric field are presented in Figures 2(a) and 2(b). When an ultraintense laser pulse interacts with under-dense plasma, the laser pulse propagates through the plasma with minimal energy loss. As shown in Figure 2(a), the bubble regime is not formed sufficiently for the LWFA of the electron acceleration scheme. Figure 2(b) shows the corresponding transverse electric field in the under-dense plasma. When the laser pulse penetrates the plasma, the ponderomotive force causes electrons to be expelled sideways. Ions form a positively charged sheath behind the laser pulse because they are not expelled as quickly as electrons. The electrons are then pulled back towards the laser axis by the electrostatic field created.

The electron and photon energy spectra are shown in Figures 2(c) and 2(d). In the electron energy spectrum, the purple line indicates the electron energy in the under-dense plasma when the laser pulse approaches the end of the under-dense plasma, and the electron energy is higher in under-dense plasma than after interacting with the rear foil. The electron energy in the under-dense target is 189 MeV. The corresponding electron energy values for Al, Cu, and Au are 85 MeV, 75 MeV, and 80 MeV, respectively. Only when these high-energy electrons from the under-dense plasma interact with the rear foil attached to the under-dense target can photon emission be enhanced. Figure 2(d) shows the photon energy for all three foils; the obtained maximum photon energy values for Al, Cu, and Au are 61.3 MeV, 116 MeV, and 149.6 MeV, respectively. The highest photon energy is found in the case of the Au target. As increasing the  $Z$  of the target, the bremsstrahlung emission increases due to the increase in the interaction cross section between the electron and the ion. The photon number from the bremsstrahlung mechanism is shown in Figure 3.

The comparison of photon numbers generated from Al, Cu, or Au indicate that the number generated by Al is

smaller than that generated by Cu and Au. The emitted photon number is found to be around  $4 \times 10^9$ ,  $4.2 \times 10^{12}$ , and  $4.5 \times 10^{13}$  for Al, Cu, and Au, respectively. The results indicate a maximum bremsstrahlung photon energy and the photon numbers for higher  $Z$  (Au). The simulation time is restricted to 300 fs, but the photon emission is expected to happen at a longer time scale. In addition, the angular distribution of photons is depicted in Figure 3. In Al target, the focused photon number along the  $\theta = 0^\circ$  is higher compared to Cu and Au. In case of Cu and Au, the emitted photons are mostly perpendicular to the laser direction, at about  $\theta = \pm 90^\circ$ . This transverse emission has also been observed by Morris, S. et al. [46]. But in the case of the Au target, the emitted photons along the transverse directions are one order of magnitude higher than the Cu target. The photon emission direction is longitudinal for Al, and in the case of Cu or Au, the photons are emitted along the transverse direction.

We have performed additional simulations to understand the role of a higher under-dense plasma density and its corresponding effect on the emission of photons. We performed simulations by setting the density of the first layer ranging from  $0.02n_c$  to  $2n_c$  keeping all simulation parameters similar except for the under-dense plasma density. Figures 4(a) and 4(b) show the electron density and electric field for the  $n_e = 2n_c$ . Due to the self-focusing effect, the laser pulse gains a smaller transverse profile and a higher peak intensity; the electrons in the under-dense plasma are highly focused compared to the  $n_e = 0.2n_c$ . The laser pulse loses its significant energy within the under-dense region for higher plasma density and less amount of the high energy electron bunch gets reflected by the foil leading to reduced photon emission. The corresponding electron and photon energy spectra are shown in Figures 4(c) and 4(d). In the electron energy spectrum, the electron energy in the under-dense plasma is taken just before interacting with the foil in both the cases  $0.2n_c$  and  $2n_c$ . The electron energy in the under-dense target is 135 MeV, and electron energy for Al, Cu, and Au is 58 MeV, 65 MeV, and 68 MeV, respectively. The photon energy is higher in the Au case than in the Al and Cu cases. The corresponding photon energy for Al, Cu, and Au is 29.1 MeV, 55.3 MeV, and 81.3 MeV, respectively.

In addition, we also looked into the photon number and distribution of the photons in different targets in Figure 5.

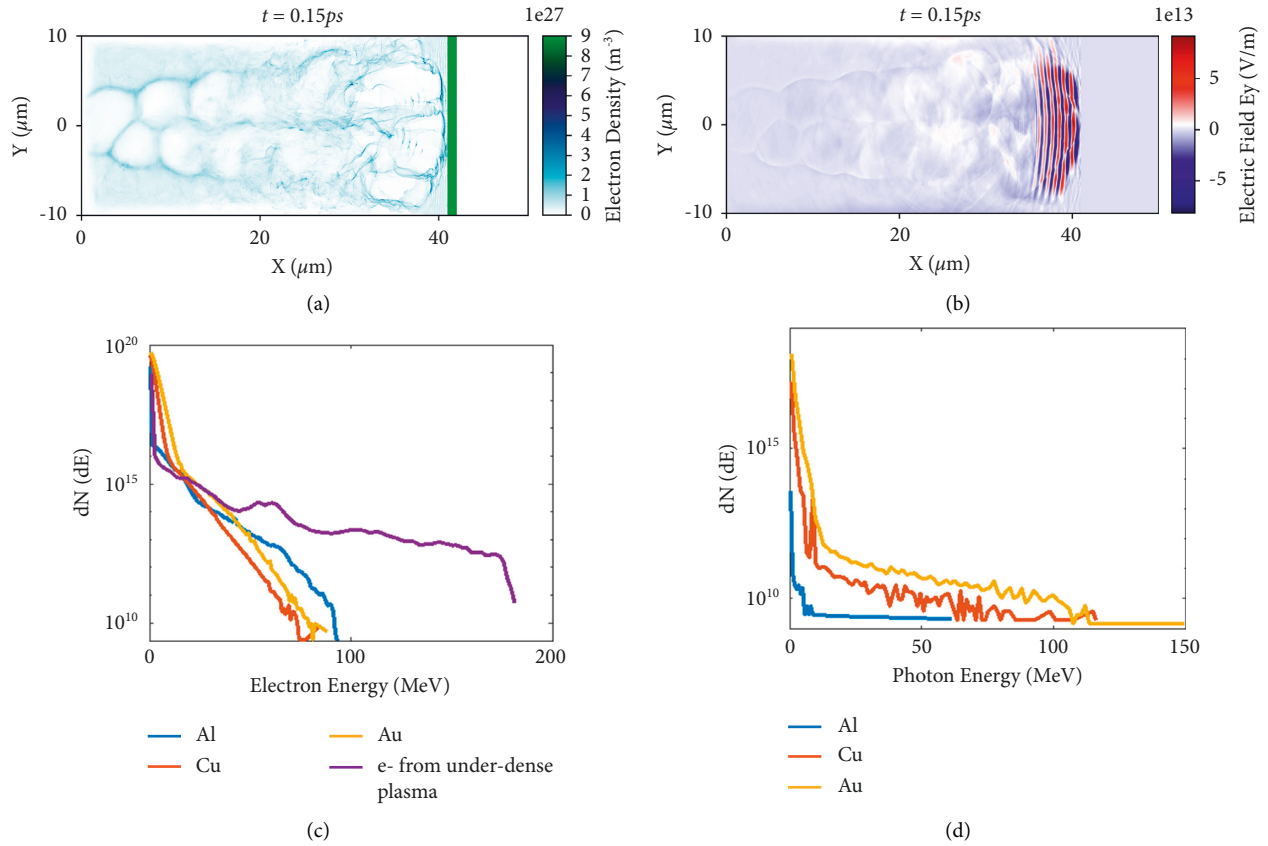


FIGURE 2: (a) Electron density distribution in under-dense plasma for  $0.2n_c$  (b) corresponding transverse electric field, (c) electron energy, and (d) photon energy spectrum for  $0.2n_c$ .

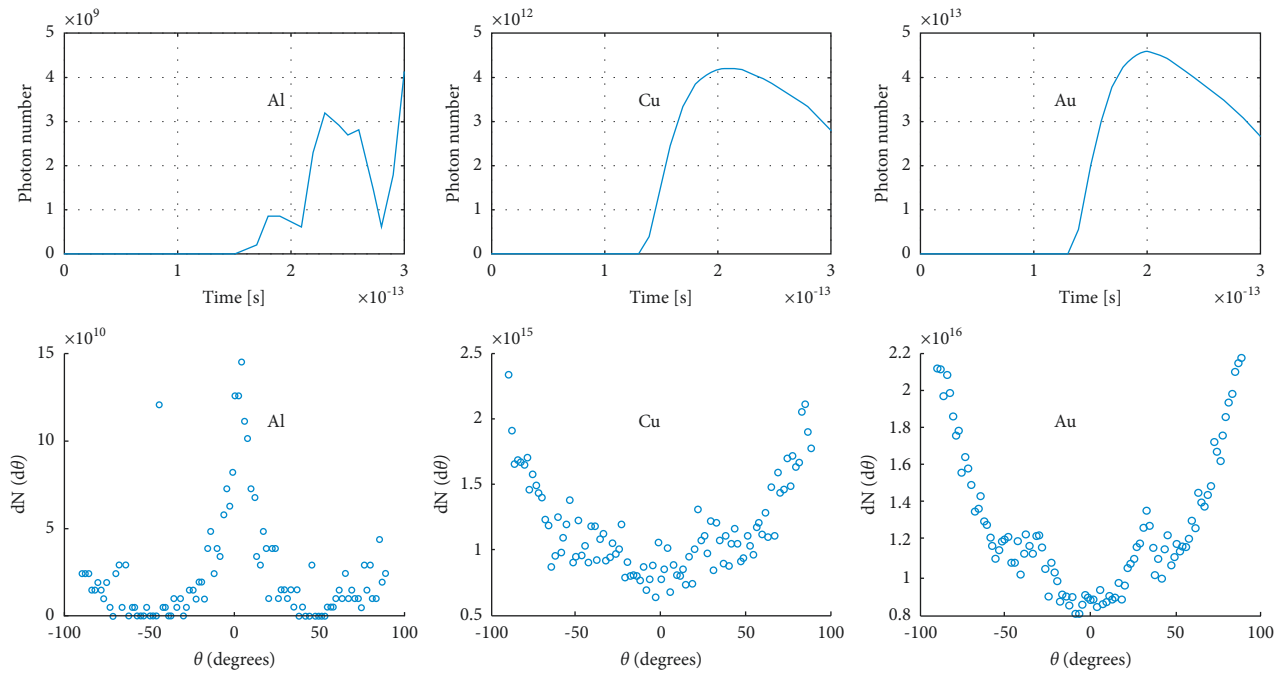


FIGURE 3: Photon number (above) and angular distribution of photons (below) for  $0.2n_c$ .

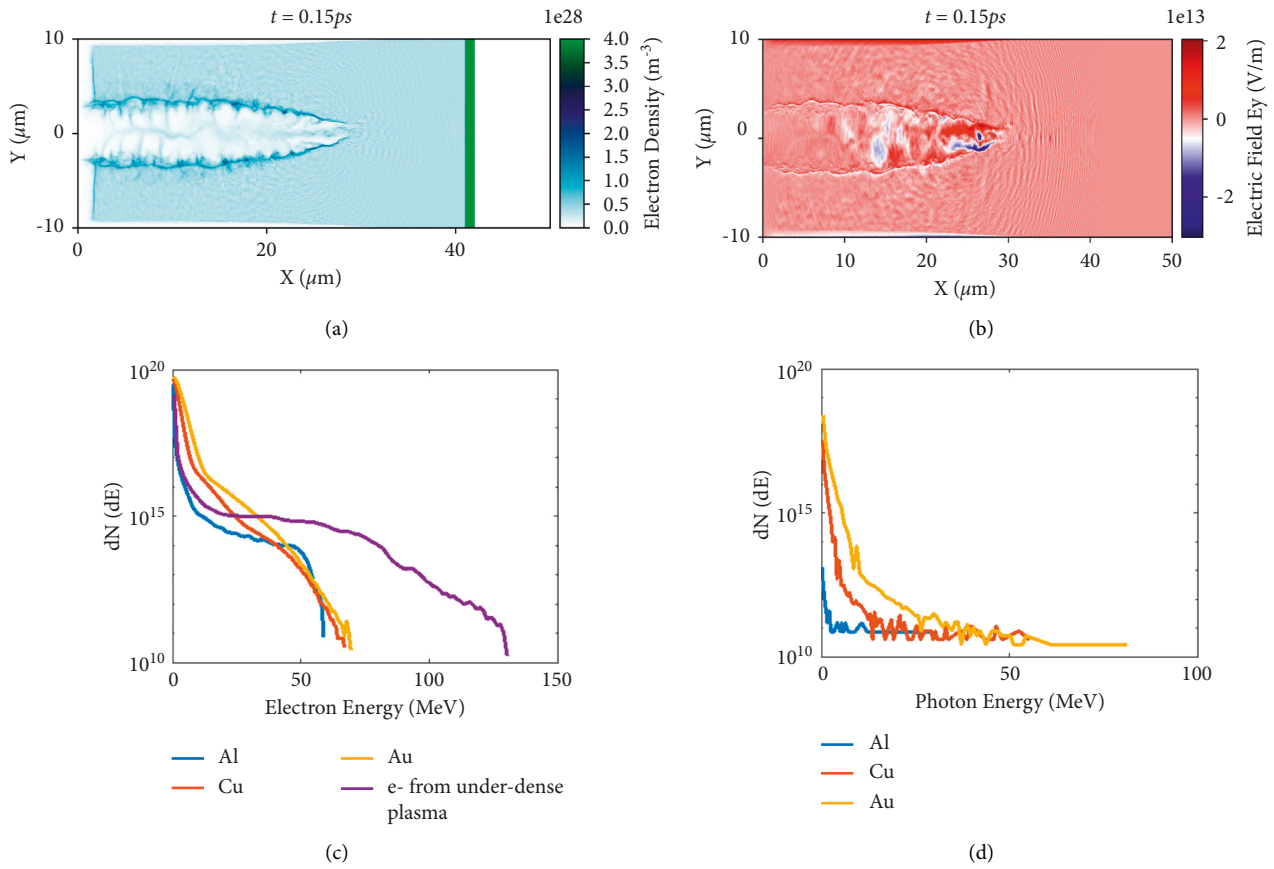


FIGURE 4: (a) Electron density distribution in under-dense plasma for  $2n_c$  (b) corresponding transverse electric field, (c) electron energy, and (d) photon energy spectrum for  $2n_c$ .

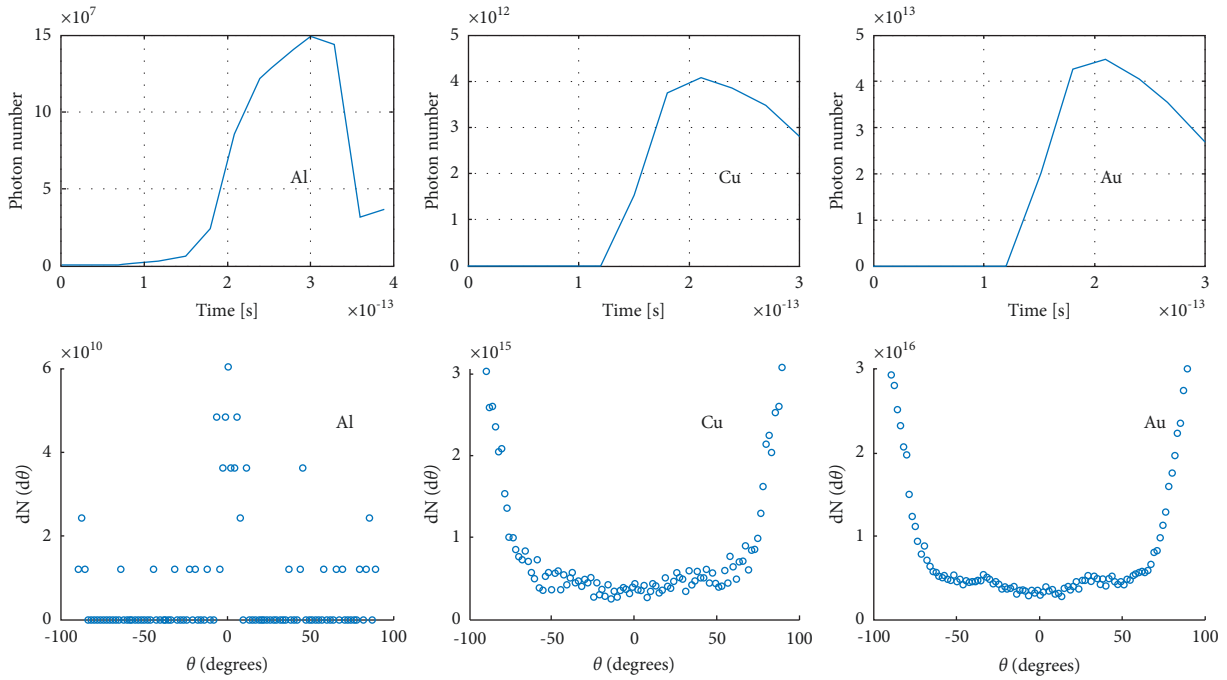


FIGURE 5: Photon number (above) and angular distribution of photons (below) for  $2n_c$ .

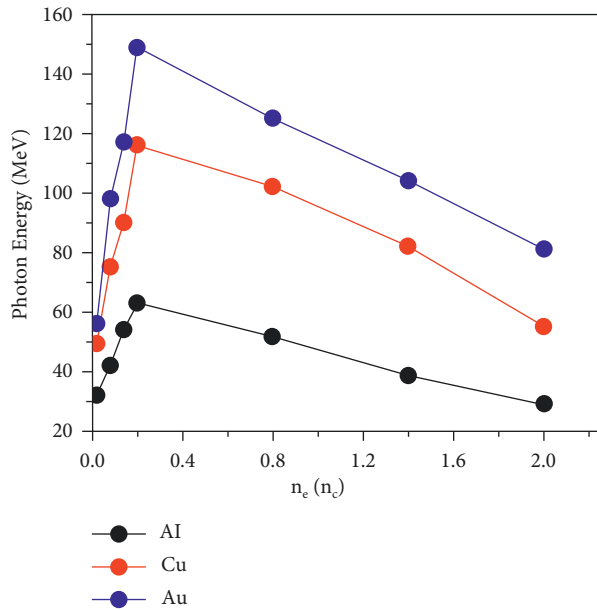


FIGURE 6: The photon energy dependency on different densities in under-dense plasma.

The emitted photon number is found to be around  $1.4 \times 10^8$ ,  $4 \times 10^{12}$ , and  $4.3 \times 10^{13}$  for Al, Cu, and Au, respectively. The generated photon number by the Al target is smaller than the Cu and Au targets. The maximum photon energy and the corresponding photons emitted are relatively higher for Au. In addition, we also depict the angular distribution of photons. In the Al target, the focused photons are relatively high compared to Cu and Au. But in the case of the Au target, the photons are comparatively higher than the Cu target. For a given laser pulse, the photon yield and energy can be affected by the parameters of under-dense plasma density. We performed a series of PIC simulations by varying the under-dense plasma density to obtain the optimal density for the highest photon yield and corresponding energy. Here, we changed the density of the under-dense plasma, but the length of the under-dense plasma is fixed to  $40 \mu\text{m}$ . The results shown in Figure 6 are the photon energy dependence on different densities in all three targets. The photon number and energy decrease with increasing under-dense plasma density. The optimal density is found to be  $n_e = 0.2n_c$ . At this density, the number and energy of the photons are high compared to other densities. If the length and density of an under-dense plasma are too small, the resulting electron energy and number are limited. When under-dense plasma is too long and too dense, filamentation may occur, and thus, the laser absorption efficiency will be reduced in hydrogen layers with a higher density. Both are disadvantageous to the generation of high-energy photons.

#### 4. Conclusion

A hybrid double-layer setup has been studied via 2D EPOCH simulations for the gamma ray production following the interaction of high intensity ( $I = 4 \times 10^{21} \text{ Wcm}^{-2}$ ) short-pulse laser. The results confirm photon energy enhancement

for Au (high Z) target with the interaction of MeV electrons driven by the laser pulse interacting with the under-dense plasma in the hybrid structure. MeV electrons are accelerated in the under-dense region through well-known laser-plasma mechanisms such as LWFA and DLA. In conclusion, our simulations suggest an improved photon beam divergence and conversion efficiency of laser energy to photons if a high Z layer is present in the hybrid target. This study will be of fundamental importance for various applications in high-intensity laser-plasma interactions.

#### Data Availability

Data will be made available from the corresponding author upon reasonable request.

#### Conflicts of Interest

The authors declare that they have no conflicts of interest.

#### Acknowledgments

The authors would like to acknowledge the EPOCH code used in this research which the University of Warwick developed as part of UK EPSRC Project No. EP/G054940/1, EP/G054950/1, EP/G056803/1, EP/G055165/1, and EP/M022463/1. The authors also acknowledge the Council of Scientific and Industrial Research (CSIR) and imprint projects (IMP/2019/000275).

#### References

- [1] D. Strickland and G. Mourou, "Compression of amplified chirped optical pulses," *Optics Communications*, vol. 56, no. 3, pp. 219–221, 1985.
- [2] C. N. Danson, C. Haefner, J. Bromage et al., "Petawatt and exawatt class lasers worldwide," *High Power Laser Science and Engineering*, vol. 7, p. e54, 2019.
- [3] T. E. Cowan, J. Fuchs, H. Ruhl et al., "Ultralow emittance, multi-MeV proton beams from a laser virtual-cathode plasma accelerator," *Physical Review Letters*, vol. 92, no. 20, Article ID 204801, 2004.
- [4] M. D. Perry, J. A. Sefcik, T. Cowan et al., "Hard x-ray production from high intensity laser solid interactions (invited)," *Review of Scientific Instruments*, vol. 70, no. 1, pp. 265–269, 1999.
- [5] S. V. Bulanov and V. S. Khoroshkov, "Feasibility of using laser ion accelerators in proton therapy," *Plasma Physics Reports*, vol. 28, no. 5, pp. 453–456, 2002.
- [6] S. V. Bulanov, T. Z. Esirkepov, M. Kando, J. Koga, K. Kondo, and G. Korn, "On the problems of relativistic laboratory astrophysics and fundamental physics with super powerful lasers," *Plasma Physics Reports*, vol. 41, no. 1, pp. 1–51, 2015.
- [7] K. Ta Phuoc, S. Corde, C. Thaury et al., "All-optical Compton gamma-ray source," *Nature Photonics*, vol. 6, no. 5, pp. 308–311, 2012.
- [8] O. J. Pike, F. Mackenroth, E. G. Hill, and S. J. Rose, "A photon-photon collider in a vacuum hohlraum," *Nature Photonics*, vol. 8, no. 6, pp. 434–436, 2014.
- [9] J. J. Honrubia, J. C. Fernández, M. Temporal, B. M. Hegelich, and J. Meyer-ter-Vehn, "Fast ignition of inertial fusion targets

- by laser-driven carbon beams,” *Physics of Plasmas*, vol. 16, no. 10, Article ID 102701, 2009.
- [10] M. Roth, T. E. Cowan, M. H. Key et al., “Fast ignition by intense laser-accelerated proton beams,” *Physical Review Letters*, vol. 86, no. 3, pp. 436–439, 2001.
- [11] A. Macchi, A. Antonicci, S. Atzeni et al., “Fundamental issues in fast ignition physics: from relativistic electron generation to proton driven ignition,” *Nuclear Fusion*, vol. 43, no. 5, pp. 362–368, 2003.
- [12] V. Tikhonchuk, Y. J. Gu, O. Klimo, J. Limpouch, and S. Weber, “Studies of laser-plasma interaction physics with low-density targets for direct-drive inertial confinement schemes,” *Matter and Radiation at Extremes*, vol. 4, no. 4, Article ID 045402, 2019.
- [13] R. Betti and O. A. Hurricane, “Inertial-confinement fusion with lasers,” *Nature Physics*, vol. 12, Article ID 435448, 2016.
- [14] R. D. Edwards, M. A. Sinclair, T. J. Goldsack et al., “Characterization of a gamma-ray source based on a laser-plasma accelerator with applications to radiography,” *Applied Physics Letters*, vol. 80, no. 12, pp. 2129–2131, 2002.
- [15] Y. Glinec, J. Faure, L. Le Dain et al., “High-resolution-ray radiography produced by a laser-plasma driven electron source,” *Physical Review Letters*, vol. 94, no. 2, Article ID 025003, 2005.
- [16] E. C. Halperin, C. A. Perez, and L. W. Brady, *Principles and Practice of Radiation Oncology*, Wolters Kluwer Health, Philadelphia, PA, USA, 2008.
- [17] T. E. Cowan, A. W. Hunt, T. W. Phillips et al., “Photonuclear fission from high energy electrons from ultraintense laser-solid interactions,” *Physical Review Letters*, vol. 84, no. 5, pp. 903–906, 2000.
- [18] S. A. Reed, V. Chvykov, G. Kalintchenko, T. Matsuoka, P. Rousseau, and V. Yanovsky, “Photonuclear fission with quasi-monoenergetic electron beams from laser wake fields,” *Applied Physics Letters*, vol. 89, no. 23, Article ID 231107, 2006.
- [19] A. Giuliotti, N. Bourgeois, T. Ceccotti et al., “Intense-ray source in the giant-dipole-resonance range driven by 10-TW laser pulses,” *Physical Review Letters*, vol. 101, no. 10, Article ID 105002, 2008.
- [20] M. Marziani, A. Taibi, G. Di Domenico, and M. Gambaccini, “Optimization of radiography applications using x-ray beams emitted by compact accelerators. part I. Monte Carlo study of the hard x-ray spectrum,” *Medical Physics*, vol. 36, no. 10, pp. 4683–4701, 2009.
- [21] G. V. Stupakov and M. S. Zolotarev, “Ponderomotive laser acceleration and focusing in vacuum for generation of attosecond electron bunches,” *Physical Review Letters*, vol. 86, no. 23, pp. 5274–5277, 2001.
- [22] D. J. Stark, T. Toncian, and A. V. Arefiev, “Enhanced multi-MeV photon emission by a laser-driven electron beam in a self-generated magnetic field,” *Physical Review Letters*, vol. 116, no. 18, Article ID 185003, 2016.
- [23] M. Schollmeier, A. B. Sefkow, M. Geissel et al., “Laser-to-hot-electron conversion limitations in relativistic laser matter interactions due to multi-picosecond dynamics,” *Physics of Plasmas*, vol. 22, no. 4, Article ID 043116, 2015.
- [24] I. Pomerantz, E. McCary, A. R. Meadows et al., “Ultrashort pulsed neutron source,” *Physical Review Letters*, vol. 113, no. 18, Article ID 184801, 2014.
- [25] C. Gahn, G. D. Tsakiris, G. Pretzler et al., “Generating positrons with femtosecond-laser pulses,” *Applied Physics Letters*, vol. 77, Article ID 26622664, 2000.
- [26] J. D. Kmetec, C. L. Gordon, J. J. Macklin, B. E. Lemoff, G. S. Brown, and S. E. Harris, “MeV x-ray generation with a femtosecond laser,” *Physical Review Letters*, vol. 68, no. 10, pp. 1527–1530, 1992.
- [27] P. A. Norreys, M. Santala, E. Clark et al., “Observation of a highly directional  $\gamma$ -ray beam from ultrashort, ultraintense laser pulse interactions with solids,” *Physics of Plasmas*, vol. 6, no. 5, pp. 2150–2156, 1999.
- [28] S. P. Hatchett, C. G. Brown, T. E. Cowan et al., “Electron, photon, and ion beams from the relativistic interaction of petawatt laser pulses with solid targets,” *Physics of Plasmas*, vol. 7, no. 5, pp. 2076–2082, 2000.
- [29] A. Ben-Ismael, O. Lundh, C. Rechatin et al., “Compact and high-quality-ray source applied to 10m-range resolution radiography,” *Applied Physics Letters*, vol. 98, no. 26, Article ID 264101, 2011.
- [30] C. S. Brady, C. P. Ridgers, T. D. Arber, A. R. Bell, and J. G. Kirk, “Laser absorption in relativistically underdense plasmas by synchrotron radiation,” *Physical Review Letters*, vol. 109, no. 24, Article ID 245006, 2012.
- [31] J. Liu, J. Yu, Y. Shou et al., “Generation of bright  $\gamma$ -ray/hard x-ray flash with intense femtosecond pulses and double-layer targets,” *Physics of Plasmas*, vol. 26, no. 3, Article ID 033109, 2019.
- [32] E. N. Nerush, I. Y. Kostyukov, L. Ji, and A. Pukhov, “Gamma-ray generation in ultrahigh-intensity laser-foil interactions,” *Physics of Plasmas*, vol. 21, no. 1, Article ID 013109, 2014.
- [33] S. Cipiccia, M. R. Islam, B. Ersfeld et al., “Gamma-rays from harmonically resonant betatron oscillations in a plasma wake,” *Nature Physics*, vol. 7, no. 11, pp. 867–871, 2011.
- [34] E. Esarey, C. B. Schroeder, and W. P. Leemans, “Physics of laser-driven plasma-based electron accelerators,” *Reviews of Modern Physics*, vol. 81, no. 3, Article ID 12291285, 2009.
- [35] W. Schumaker, G. Sarri, M. Vargas et al., “Measurements of high-energy radiation generation from laser-Wakefield accelerated electron beams,” *Physics of Plasmas*, vol. 21, no. 5, Article ID 056704, 2014.
- [36] A. Di Piazza, C. Müller, K. Z. Hatsagortsyan, and C. H. Keitel, “Extremely high-intensity laser interactions with fundamental quantum systems,” *Reviews of Modern Physics*, vol. 84, no. 3, pp. 1177–1228, 2012.
- [37] D. W. Forslund, J. M. Kindel, and K. Lee, “Theory of hot-electron spectra at high laser intensity,” *Physical Review Letters*, vol. 39, no. 5, pp. 284–288, 1977.
- [38] W. L. Kruer and K. Estabrook, “ $J \times B$  heating by very intense laser light,” *Physics of Fluids*, vol. 28, no. 1, pp. 430–432, 1985.
- [39] F. Brunel, “Not-so-resonant, resonant absorption,” *Physical Review Letters*, vol. 59, no. 1, pp. 52–55, 1987.
- [40] H. W. Koch and J. W. Motz, “Bremsstrahlung cross-section formulas and related data,” *Reviews of Modern Physics*, vol. 31, no. 4, pp. 920–955, 1959.
- [41] T. Tajima and J. M. Dawson, “Laser electron accelerator,” *Physical Review Letters*, vol. 43, no. 4, pp. 267–270, 1979.
- [42] M. Jirka, O. Klimo, Y. J. Gu, and S. Weber, “Enhanced photon emission from a double-layer target at moderate laser intensities,” *Scientific Reports*, vol. 10, p. 8887, 2020.
- [43] H. Y. Wang, X. Q. Yan, J. E. Chen et al., “Efficient and stable proton acceleration by irradiating a two-layer target with a linearly polarized laser pulse,” *Physics of Plasmas*, vol. 20, no. 1, Article ID 013101, 2013.
- [44] A. Pukhov, Z. M. Sheng, and J. Meyer-ter-Vehn, “Particle acceleration in relativistic laser channels,” *Physics of Plasmas*, vol. 06, p. 2847, 1999.

- [45] C. Gahn, G. D. Tsakiris, A. Pukhov et al., “Multi-mev electron beam generation by direct laser acceleration in high-density plasma channels,” *Physical Review Letters*, vol. 83, p. 4772, 1999.
- [46] S. Morris, A. Robinson, and C. Ridgers, “Highly efficient conversion of laser energy to hard x-rays in high-intensity laser-solid simulations,” *Physics of Plasmas*, vol. 28, no. 10, Article ID 103304, 2021.
- [47] S. Chintalwad, S. Krishnamurthy, B. Ramakrishna, and C. P. Ridgers, “Photon emission enhancement studies from the interaction of ultra-intense laser pulses with shaped targets,” *Physical Review E—Statistical Physics, Plasmas, Fluids, and Related Interdisciplinary Topics*, vol. 105, Article ID 025205, 2022.
- [48] K. and Motz, “Bremsstrahlung cross-section formulas and related data,” *Reviews of Modern Physics*, vol. 31, 1959.
- [49] Y.-S. Tsai, “Pair production and bremsstrahlung of charged leptons,” *Reviews of Modern Physics*, vol. 46, no. 4, pp. 815–851, 1974.
- [50] T. D. Arber, K. Bennett, C. S. Brady et al., “Contemporary particle-in-cell approach to laser-plasma modelling,” *Plasma Physics and Controlled Fusion*, vol. 57, no. 11, Article ID 113001, 2015.